DE GRUYTER
Biomed. Eng.-Biomed. Tech. 2016; 61(4): 455–461

Minmin Luo, Can Hu, Yayun Zhuang, Wufan Chen, Feng Liu and Sherman Xuegang Xin*

Numerical assessment of the reduction of specific absorption rate by adding high dielectric materials for fetus MRI at 3 T

DOI 10.1515/bmt-2015-0171
Received March 12, 2015; accepted February 17, 2016; online first March 17, 2016

Abstract: The specific absorption rate (SAR) is an important issue to be considered in fetus MRI at 3 T due to the high radiofrequency energy deposited inside the body of pregnant woman. The high dielectric material (HDM) has shown its potential for enhancing B_1 field and reducing SAR in MRI. The aim of this study is to assess the feasibility of SAR reduction by adding an HDM to the fetus MRI. The feasibility of SAR reduction is numerically assessed in this study, using a birdcage coil in transmission loaded with an electromagnetic pregnant woman model in the SEMCAD-EM solver. The HDMs with different geometric arrangements and dielectric constants are manually optimized. The B_1^+ homogeneity is also considered while calculating the optimized fetus 10 g local SAR among different strategies in the application of HDM. The optimum maximum fetus 10 g local SAR was obtained as 2.25 W/kg, by using two conformal pads placed left and right with the dielectric constant to be 400, reduced by 24.75% compared to that without the HDM. It indicated that the SAR can be significantly reduced with strategic placement of the HDM and the use of HDM may provide a simple, effective and low-cost method for reducing the SAR for the fetus MRI at 3 T.

Keywords: fetus magnetic resonance imaging; finite-difference time-domain; high dielectric material; pregnant woman pelvis model; radiofrequency field; specific absorption rate.

***Corresponding author: Sherman Xuegang Xin,** Biomedical Engineering Institute of Southern Medical University, 510515 Guangzhou, China, E-mail: shermansheen@gmail.com
Minmin Luo, Can Hu, Yayun Zhuang and Wufan Chen: Biomedical Engineering Institute of Southern Medical University, 510515 Guangzhou, China
Feng Liu: School of Information Technology and Electrical Engineering of Queensland University, 4702 Brisbane, Australia

Introduction

Clinical applications of magnetic resonance imaging (MRI) for the examination of the human fetus have been substantially developed since the first attempt in the 1980s [21]. A review of current literature supports the following conclusions for a fetus MRI: a fetus MRI is very useful in the situations where suspected central nervous system anomalies, neck and oropharyngeal masses, diaphragmatic hernia, abdominal masses, bowel pathology, and fetal infection might not be fully characterized by ultrasonography [2, 13, 24]. Furthermore, fetus MRI has advantages for demonstrating pathology of the brain, lungs, complex syndromes and conditions related to the reduction of amniotic fluids [1, 20].

Commercially-available whole-body magnetic resonance scanners operating at higher magnetic field strengths, such as 3 T, are now becoming popular, because of the higher signal-to-noise ratio they offer over low-field strength scanners. This, in turn, enables the acquisition of images at higher temporal and/or higher spatial resolutions, compared to those at 1.5 T. Images at such resolutions may help in improving the diagnostic accuracy for a wide variety of pathologies [3, 4, 26]. Though the fetus MRI has mainly been clinically performed at 1.5 T, some research is currently underway to take advantage of the attractive benefits of fetus MRI at 3 T [18, 19]. Despite obvious improvements in the image quality at 3 T, the specific absorption rate (SAR) usually increases significantly at the same time [12], which is the top priority concern of safety for the fetus [10, 27, 29]. Increased SAR results in increased tissue temperatures, which may be very harmful during pregnancy if they are above the safety level, with the higher probability of embryonic death, abortion, growth retardation and developmental defects [9]. Furthermore, tissue temperature increases may also cause a wide range of structural and functional defects [8].

Recently published reports have demonstrated that the appropriate placement of the high dielectric material (HDM) between the human tissues and RF coil is able

to reduce the SAR to some extent. This is because of the enhancement of the B_1 field for a given input power in the regions that are surrounded by the HDM [16, 25]. The B_1 field distribution of the coil is altered by the strong displacement currents caused by the existence of the HDM, resulting in stronger B_1 fields in the region of interest (ROI) [30, 32]. As a direct result, the average SAR levels in the ROI are simultaneously decreased, because of the decreased input RF power [31]. Yang et al. [31] showed that the use of an HDM surrounding the human head could reduce the required input radiofrequency power by 50% throughout the cerebrum at 3 T. Brink et al. [5] also proved that the HDM did not introduce any additional RF hot spots; furthermore, the SAR is substantially reduced because of the localized increase in transmit efficiency. However, the potential merit of using HDM for the reduction of SAR in a fetus MRI at 3 T is not reported in the literature. It will be meaningful to explore the strategy of selection and placement of HDM for the reduction of the SAR in fetus MRI. In this study, the potential merit of using HDM for the reduction of SAR in a fetus MRI at 3 T is numerically explored. The results showed that the appropriate arrangement of the HDM can improve the safety of fetus MRI at 3 T in terms of the reduced SAR.

Materials and methods

Coil Model

A 16 rung body-size (diameter, 60 cm; length, 40 cm; shield diameter, 68 cm; length, 100 cm) shielded high-pass birdcage coil was modeled. Thirty-two current sources placed in the top and bottom end-rings were used to perform the function of the capacitors. The current sources had the same amplitude but their phases were equal to the azimuthal angles. The coil was driven by two voltage sources, one source was set in the inferior end-ring, with a phase of 180 degree shifted from that of the other source at the same location in the superior end-ring, resulting in an ideal current distribution for a homogeneous B_1 field [11, 14].

Table 1: Dielectric parameters and mass densities of different tissues in the pregnant woman pelvis model at 3T.

Tissue	Conductivity (S/m)	Relative dielectric constant	Density (kg/m³)
Bone	0.18	26.284	1357
Fat	0.037	5.922	916
Muscle	0.719	63.495	1040
Uterus	0.961	75.433	1050
Skin	0.523	65.437	1125
Placenta	0.719	63.495	1027
Amniotic fluid	2.143	84.041	1000
Fetal body	1.242	76.451	1040
Fetal brain	0.932	67.451	1030

Pregnant woman pelvis model

An established adult female pelvis model, the same as that used in [28], was used to generate a pregnant woman pelvis model by merging a numerical fetal model into it. The numerical fetal model came from the report of Chen [6], which was a fetus model at 13 weeks. In this research, the total mass of the model is 12.7272 kg. The fetus was attached to the uterus wall by the placenta. The placenta was placed next to the uterine wall in the upper hemisphere of the uterine, and the fetus was set to facedown. Corresponding dielectric parameters and mass densities, listed in Table 1, were assigned to different tissues in the established pregnant woman pelvis model. It was assumed that the dielectric properties of the placenta and amniotic fluid respectively were the same as that of the muscle and cerebrospinal fluid. The pregnant woman pelvis model was geometrically set at the center of the birdcage coil.

HDM models

The application of the HDM was manually optimized with different geometric arrangements in the simulations, including, (1) two rectangular pads with a thickness of 10 mm placed left and right of the pelvis model (Figure 1A), (2) two conformal pads with a thickness of 10 mm placed left and right of the pelvis model (Figure 1B) and (3) two conformal pads with a thickness of 10 mm placed anterior and posterior of the pelvis model (Figure 1C). A distance of 1 mm was set to maintain the space for the plastic encasing of the dielectric material and the subject's clothing. By reason of implementing

Figure 1: HDM placed around the pregnant woman pelvis model, (A) two rectangular pads placed left and right, dimensions of each pad: area, 200×200 mm²; thickness, 10 mm; (B) two conformal pads placed left and right, dimensions of each pad: area, 240×200 mm²; thickness, 10 mm; (C) two conformal pads placed anterior and posterior, dimensions of each pad: area, 200×200 mm²; thickness, 10 mm.

this separation distance, the mesh resolution was increased to 1 mm around the pads [5].

EM simulations

The commercially-available software package SEMCAD X (Schmid & Partner Engineering AG, Zurich, Switzerland) was used to calculate the electromagnetic fields. The kernel of SEMCAD was built using the finite-difference time-domain (FDTD) method that is able to effectively solve with high accuracy the electromagnetic fields that interact with irregularly shaped inhomogeneous loads [22]. Eight perfectly-matched layers were used as the boundary conditions [23]. The three-dimensional mesh with isometric 2.5 mm resolution was created in all simulations. The dielectric constant of the HDM used in the simulations was optimized manually with a step of 100. The conductivity of the HDM was assumed as 0.35 S/m (when the relative dielectric constant was set equal/<500), or 0.5 S/m (when the relative dielectric constant was set equal/above 600) [5, 15, 16]. The post-processing of the simulation results was performed in MATLAB (The Mathworks, Natick, MA, USA). The partial body SAR, maximum mother 10 g local SAR and maximum fetus 10 g local SAR were all calculated. All SAR values were normalized to a B_1^+ field intensity of 1.957 μT in the ROI (the region where the fetus was located); this is the field intensity required to produce a flip angle of 90° with a 3 ms rectangular RF pulse [7].

Results

The partial body average SAR, maximum mother 10 g local SAR and maximum fetus 10 g local SAR within the whole pelvis model using different geometric HDMs with various dielectric constants were shown in Table 2. The partial body SAR, maximum mother 10 g local SAR and maximum fetus 10 g local SAR without HDM were 1.89, 12.95 and 2.99 W/kg, respectively. The deviations of the SAR values between with and without the HDM were calculated as:

$$SAR_{Deviation} = \frac{SAR_{HDM} - SAR_{no\ HDM}}{SAR_{no\ HDM}} \times 100\% \quad (1)$$

The optimum dielectric constant of two rectangular pads placed left and right of the pelvis model was found to be about 500, meanwhile the partial body SAR, maximum mother 10 g local SAR and maximum fetus 10 g local SAR were 1.56, 4.87 and 2.78 W/kg, respectively. The optimum dielectric constant of two conformal pads placed left and right of the pelvis model was found to be about 400; meanwhile, the partial body SAR, maximum mother 10 g local SAR and maximum fetus 10 g local SAR were 1.35, 5.3 and 2.25 W/kg, respectively. The optimum dielectric constant of two conformal pads placed anterior and posterior of the pelvis model was found to be about 600; meanwhile the partial body SAR, maximum mother 10 g local SAR and maximum fetus 10 g local SAR were 1.76, 9.04 and 2.36 W/kg, respectively. The SAR distributions in different geometric situations with the optimum selection of dielectric constant are shown in Figure 2.

Discussion

The results showed that the SAR values first decreased and then increased, while the dielectric constant varied from 100 to 1000. Among the three geometric arrangements, the optimum maximum fetus 10 g local SAR was found to be 2.25 W/kg, reduced by 24.75% compared to that without HDM where two conformal pads were placed left and right with the dielectric constant of 400, indicating the optimum geometric arrangement of the HDM. Furthermore, the maximum mother 10 g local SAR without HDM was found to be 12.95 W/kg; this did not meet the requirement of IEC, indicating a high risk of SAR safety for a pregnant woman undergoing an MR scan at 3 T. The maximum mother 10 g local SAR could be significantly reduced using HDM with appropriate dielectric constant. In the optimum case, the maximum mother 10 g local SAR was found to be 5.3 W/kg and the optimum maximum fetus 10 g local SAR was found to be 2.25 W/kg, thus meeting the requirement of the IEC standard (10 W/kg) [17]. Inside the entire pelvis model, the peaks of the local SARs appeared in skin, muscle and fetus (Figure 2). This can be significantly reduced with the optimum arrangement of the HDM. In addition, no new hotspots were found by adding the HDM.

The situations using various thicknesses of the HDM were explored in this study. Three different geometric HDMs (Figure 1) with a thickness of 5 mm were simulated. The optimum dielectric constant of two rectangular pads with a thickness of 5 mm placed left and right of the pelvis model was found to be about 500; meanwhile, the partial body SAR, maximum mother 10 g local SAR and maximum fetus 10 g local SAR were 1.65, 7.34 and 2.83 W/kg, respectively. The optimum dielectric constant of the two conformal pads with a thickness of 5 mm placed left and right of the pelvis model was found to be about 400; meanwhile, the partial body SAR, maximum mother 10 g local SAR and maximum fetus 10 g local SAR were 1.75, 7.19 and 2.45 W/kg, respectively. The optimum dielectric constant of the two conformal pads with a thickness of 5 mm placed anterior and posterior of the

Table 2: Partial body SAR, maximum mother 10 g local SAR, maximum fetus 10 g local SAR and deviations using different geometric HDMs with various dielectric constants at 3 T.

	100	200	300	400	500	600	700	800	900	1000
Rectangular pads placed left and right										
Partial body SAR (W/kg)	1.78	1.62	1.57	1.55	1.56	1.61	1.81	3.22	3.77	3.98
Deviation (%)	-5.82	-14.29	-16.93	-17.99	-17.46	-14.81	-4.23	+70.37	+99.47	+110.58
Maximum mother 10 g local SAR (W/kg)	11.67	7.77	6.77	5.45	4.87	5.53	7.6	18.86	21.03	31.45
Deviation (%)	-9.88	-40	-47.72	-57.92	-62.39	-57.3	-41.31	+45.64	+62.39	+142.86
Maximum fetus 10 g local SAR (W/kg)	2.88	2.85	2.81	2.79	2.78	2.82	2.95	3.58	3.40	3.38
Deviation (%)	-3.68	-4.68	-6.02	-6.69	-7.02	-5.69	-1.34	+19.73	+13.71	+13.04
Conformal pads placed left and right										
Partial body SAR (W/kg)	2.23	1.83	1.79	1.35	1.79	1.93	2.41	6.17	6.04	5.84
Deviation (%)	+17.99	-3.17	-5.29	-28.57	-5.29	+2.12	+27.51	+226.46	+219.58	+208.99
Maximum mother 10 g local SAR (W/kg)	17.27	11.03	8.26	5.3	6.47	8.43	14.57	63.22	68.35	72.65
Deviation (%)	+33.36	-14.83	-36.22	-59.07	-50.04	-34.9	+12.51	+388.19	+427.80	+461
Maximum fetus 10 g local SAR (W/kg)	3.03	2.92	2.90	2.25	2.96	3.12	3.48	5.77	3.68	3.63
Deviation (%)	+1.34	-2.34	-3.01	-24.75	-1	+4.35	+16.39	+92.98	+23.08	+21.4
Conformal pads placed anterior and posterior										
Partial body SAR (W/kg)	2.08	2.04	1.95	1.88	1.79	1.76	2.17	2.94	2.55	3.19
Deviation (%)	+10.05	+7.94	+3.17	-5.29	-5.29	-6.88	+14.81	+55.56	+34.92	+68.78
Maximum mother 10 g local SAR (W/kg)	18.23	15.76	12.51	10.89	10.65	9.04	11.52	19.43	17.73	32.58
Deviation (%)	+40.77	+21.7	-3.4	-15.91	-17.76	-30.19	-11.04	+50.04	+36.91	+151.58
Maximum fetus 10 g local SAR (W/kg)	2.51	2.38	2.41	2.55	2.45	2.36	2.98	2.93	5.10	6.78
Deviation (%)	-16.05	-17.39	-19.4	-14.72	-18.06	-21.07	-0.33	-2.01	+70.57	+126.76

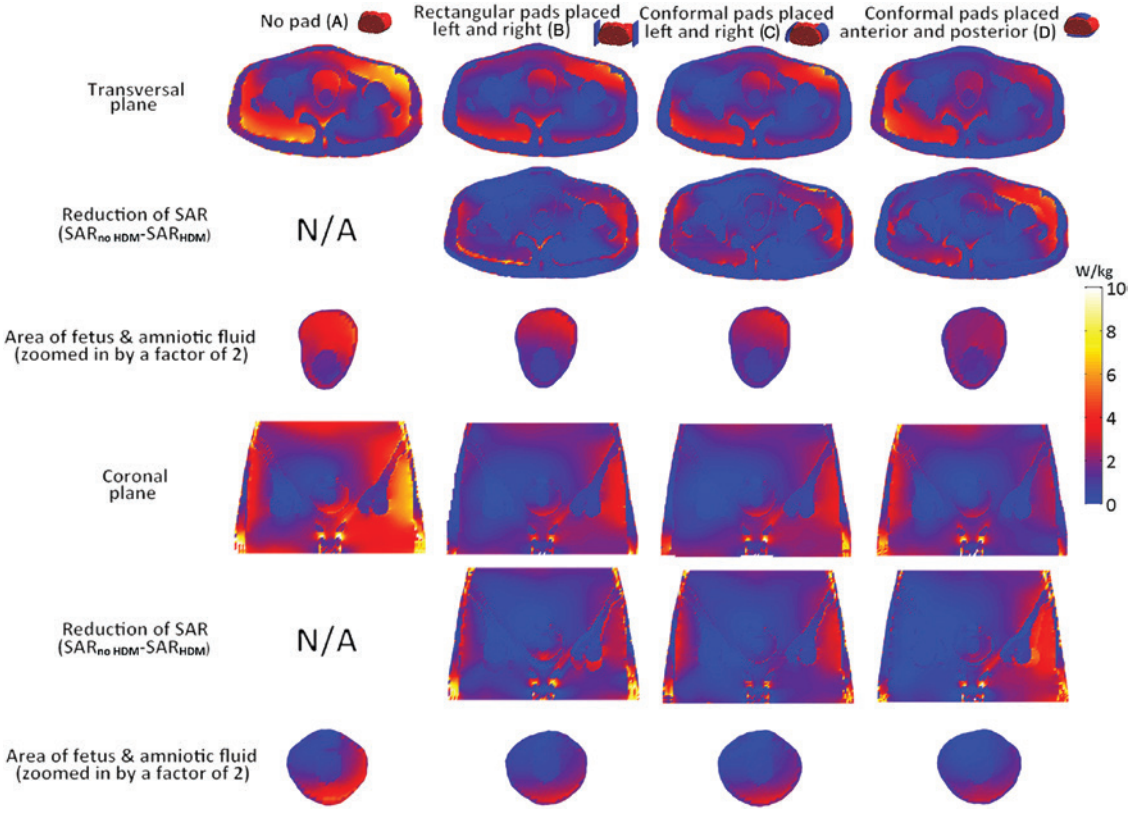

Figure 2: The shaded plots of various SAR distributions, (A) with no HDM, (B) a rectangular HDM placed left and right with the optimum dielectric constant of 500, (C) a conformal HDM placed left and right with the optimum dielectric constant of 400, and (D) a conformal HDM placed anterior and posterior with the optimum dielectric constant of 600. The reductions of the SAR on the transversal plane were (B) 16.42%, (C) 26.51% and (D) 17.26%. The reductions of the SAR on the coronal plane were (B) 18.92%, (C) 29.17% and (D) 18.33%.

pelvis model was found to be about 600; meanwhile, the partial body SAR, maximum mother 10 g local SAR and maximum fetus 10 g local SAR were 2.02, 12.33 and 2.89 W/kg, respectively. Compared with the corresponding SARs obtained using 10 mm-thickness pads, the optimum maximum fetus 10 g local SAR were increased by 1.8%, 8.89% and 22.46%, respectively. These results indicated that using an HDM with a thickness of 10 mm was better than using an HDM with a thickness of 5 mm with respect to the reduction of the fetus local SAR. The B_1^+ field homogeneity in the ROI was considered in the cases without and with an HDM having a thickness of 10 mm. The normalized B_1^+ fields on the transversal planes using an HDM with the obtained optimum dielectric constant, that is, 500, 400, 600, respectively in the three different situations, were calculated and compared to those without pads, as shown in Figure 3. The relative standard deviation (RSD) in the ROI was calculated as:

$$\mathrm{RSD}=\frac{\sigma}{\mu}\times 100\% \tag{2}$$

where σ is the standard deviation of the B_1^+ field in the ROI, which was calculated as:

$$\sigma=\sqrt{\frac{1}{N\text{-}1}\sum_{\mathrm{ROI}}\left(\left|B_1^+(r)\text{-}\mu\right|\right)^2} \tag{3}$$

and μ is the mean value of the B_1^+ field at the position r in the ROI, which was calculated as:

$$\mu=\frac{1}{N}\sum_{\mathrm{ROI}}\left|B_1^+(r)\right| \tag{4}$$

where N is the number of Yee cells in the ROI. The results indicated that the interference on the B_1^+ field homogeneity with the HDM present was negligible.

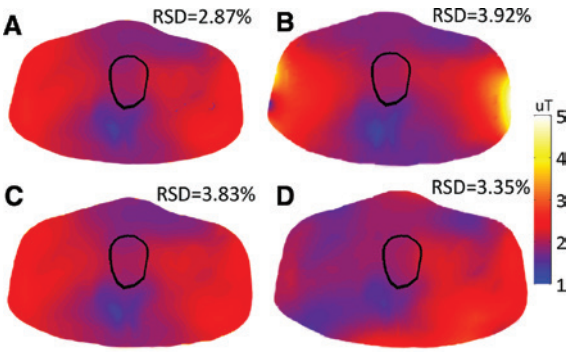

Figure 3: Shaded plots of normalized $|B_1^+|$ (the magnitude of $|B_1^+|$ field) field on transverse plane, (A) without an HDM, (B) with a rectangular HDM with a thickness of 10 mm placed left and right with the dielectric constant of 500, (C) a conformal HDM with a thickness of 10 mm placed left and right with the dielectric constant of 400, and (D) a conformal HDM with a thickness of 10 mm placed anterior and posterior with the dielectric constant of 600. The RSDs within the region of ROI are indicated in each plot.

The contribution to the B_1 field and SAR from the conductivity of HDM was much less than that from the relative dielectric constant due to the low ratio of conduction to displacement current [25], however, the conductivity does vary with different relative dielectric constant in different HDM. To further explore the influence of the variances of conductivity of HDM on B_1 field and SAR, the simulation was implemented as follows: relative dielectric constant set as 515, conductivity varied from 0.1 to 0.6 S/m with a step of 0.1 S/m. The obtained B_1 field and SAR distribution were compared with those when the conductivity was set as 0.35 S/m [16]. The results indicated that the influence of the variances of conductivity was negligible (Figure 4).

The truncated pregnant woman model merged with the mathematical fetus model was used in this study, inevitably resulting in deviations compared to the practical

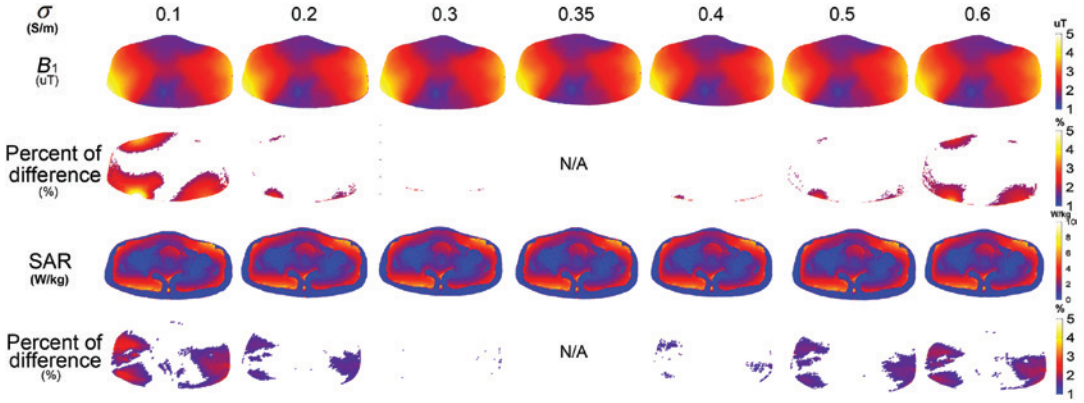

Figure 4: The shaded plots of normalized $|B_1^+|$ (the magnitude of B_1^+ field) field and SAR on the transverse plane using HDM with ε_r of 515 and various conductivity values.

Table 3: Comparison of the obtained SAR results with the data in the published literature.

Tissue	10 g local SAR in this work (W/kg)	SAR values in [27] (W/kg)
Bone	5.862	6
Fat	13.704	N/A
Muscle	9.982	N/A
Uterus	2.432	2.1
Skin	9.963	N/A
Placenta	2.135	2
Amniotic fluid	3.164	2
Fetal body	1.997	2
Fetal brain	1.875	2

fetus MRI. To verify the obtained results in this simulation, the result of SAR was compared with the data in reference [27] (Figure 8 in this reference) using the same normalization method (normalized to the whole-body averaged SAR of 2 W/kg), listed in Table 3. The result demonstrated that the obtained 10 g local SAR values of different tissues using our model without HDM were consistent with the data in [27], indicating the reliable simulation results in this work. Generally speaking, the results obtained here could obviously indicate the trend of the SAR values while undergoing a fetus MR scan with HDM. The whole body model of a pregnant woman was needed to more precisely explore the merit of the HDM in terms of the reduction of SAR in the future. The weight of HDM located anterior to the pregnant woman must to be considered. It might weigh several kilograms. It might be helpful to accommodate for a pregnant woman undergoing an MRI examination if a light HDM could be designed. From an operational point-of-view, some vendors might not include a provision for external devices, such as an HDM to reduce SAR within their strict legal terms of an insurable operation.

Conclusion

Based on our numerical study, we conclude that, the SAR can be significantly reduced with the strategic placement of an HDM with optimum dielectric constant in fetus MRI at 3 T. With further research, the use of the HDM may provide a simple, effective and low-cost method for reducing the SAR for the fetus MRI at 3 T.

Acknowledgments: This study was partially supported by the National Natural Science Foundation of China (grant number 61172034, 61528102), Science and Technology Program of Guangzhou, China (No.2014J4100160), Science and Technology Program of Guangdong, China (No.2015B020214006), Guangdong Natural Science Foundation (No. 2015A030313234). The authors would like to thank those anonymous reviewers for their constructive comments and suggestions, which have greatly improved the quality of this paper.

References

[1] Alamo L, Reinberg O, Vial Y, Gudinchet F, Meuli R. Comparison of foetal US and MRI in the characterisation of congenital lung anomalies. Eur J Radiol 2013; 82: e860–e866.
[2] Bahado-Singh RO, Goncalves LF. Techniques, terminology, and indications for MRI in pregnancy. Semin Perinatol 2013; 37: 334–339.
[3] Bi X, Li D. Coronary arteries at 3.0 T: contrast-enhanced magnetization-prepared three-dimensional breathhold MR angiography. J Magn Reson Imaging 2005; 21: 133–139.
[4] Bloch BN, Rofsky NM, Baroni RH, Marquis RP, Pedrosa I, Lenkinski RE. 3 Tesla magnetic resonance imaging of the prostate with combined pelvic phased-array and endorectal coils: Initial experience1.Acad Radiol 2004; 11: 863–867.
[5] Brink WM, Webb AG. High permittivity pads reduce specific absorption rate, improve B1 homogeneity, and increase contrast-to-noise ratio for functional cardiac MRI at 3 T. Magn Reson Med 2014; 71: 1632–1640.
[6] Chen J. Mathematical models of the embryo and fetus for use in radiological protection. Health Phys 2004; 86: 285–295.
[7] Collins CM, Smith MB. Calculations of B1 distribution, SNR, and SAR for a surface coil adjacent to an anatomically-accurate human body model. Magn Reson Med 2001; 45: 692–699.
[8] Edwards MJ. Review: hyperthermia and fever during pregnancy. Birth Defects Res A Clin Mol Teratol 2006; 76: 507–516.
[9] Edwards M, Saunders R, Shiota K. Effects of heat on embryos and foetuses. Int J Hyperthermia 2003; 19: 295–324.
[10] Hand JW, Li Y, Thomas EL, Rutherford MA, Hajnal JV. Prediction of specific absorption rate in mother and fetus associated with MRI examinations during pregnancy. Magn Reson Med 2006; 55: 883–893.
[11] Hayes CE, Edelstein WA, Schenck JF, Mueller OM, Eash M. An Efficient, Highly Homogeneous Radiofrequency Coil for Whole-Body NMR Imaging at 1.5T. J Magn Reson 1985; 63: 622–628.
[12] Kataoka M, Isoda H, Maetani Y, et al. MR imaging of the female pelvis at 3 Tesla: evaluation of image homogeneity using different dielectric pads. J Magn Reson Imaging 2007; 26: 1572–1577.
[13] Leruez-Ville M, Sellier Y, Salomon LJ, Stirnemann JJ, Jacquemard F, Ville Y. Prediction of fetal infection in cases with cytomegalovirus immunoglobulin M in the first trimester of pregnancy: a retrospective cohort. Clin Infec Dis 2013; 56: 1428–1435.
[14] Liu W, Collins CM, Smith MB. Calculations of B 1 distribution, specific energy absorption rate, and intrinsic signal-to-noise ratio for a body-size birdcage coil loaded with different human subjects at 64 and 128 MHz. Appl Magn Reson 2005; 29: 5–18.
[15] Luo W, Ryu YC, Oh S, et al. Improved material for passive RF shimming with dielectric pads. Proc Soc Mag Reson Med 2012; 20: 2700.

[16] Luo W, Michael TL, Christopher TS, et al. Permittivity and performance of dielectric pads with sintered ceramic beads in MRI: early experiments and simulations at 3 T. Magn Reson Med 2013; 70: 269–275.
[17] Medical Electrical Equipment: Part 2–33: Particular Requirements for the Basic Safety and Essential Performance of Magnetic Resonance Equipment for Medical Diagnosis. IEC 60601-2-33, 2010.
[18] Neelavalli J, Jella PK, Krishnamurthy U, et al. Measuring venous blood oxygenation in fetal brain using susceptibility-weighted imaging. J Magn Reson Imaging 2014; 39: 998–1006.
[19] Neelavalli J, Mody S, Yeo L, et al. MR venography of the fetal brain using susceptibility weighted imaging. J Magn Reson Imaging 2014; 40: 949–957.
[20] Pugash D, Brugger PC, Bettelheim D, Prayer D. Prenatal ultrasound and fetal MRI: The comparative value of each modality in prenatal diagnosis. Eur J Radiol 2008; 68: 214–226.
[21] Smith F, Adam A, Phillips W. NMR imaging in pregnancy. Lancet 1983; 321: 61–62.
[22] Taflove A. Review of the formulation and applications of the finite-difference time-domain method for numerical modeling of electromagnetic wave interactions with arbitrary structures. Wave Motion 1988; 10: 547–582.
[23] Taflove A, Hagness SC. Computational electrodynamics. Artech House: Boston 2000; 10: 547–582.
[24] Victoria T, Danzer E, Scott Adzick N. Use of ultrasound and MRI for evaluation of lung volumes in fetuses with isolated left congenital diaphragmatic hernia. Semin Pediatr Surg 2013; 22: 30–36.
[25] Webb A. Dielectric materials in magnetic resonance. Concept Magnetic Reson A 2011; 38: 148–184.
[26] Willinek WA, Born M, Simon B, et al. Time-of-Flight MR Angiography: Comparison of 3.0-T Imaging and 1.5-T Imaging – Initial Experience. Radiology 2003; 229: 913–920.
[27] Wu D, Shamsi S, Chen J, Kainz, W. Evaluations of specific absorption rate and temperature increase within pregnant female models in magnetic resonance imaging birdcage coils. IEEE Trans Microw Theory Tech 2006; 54: 4472–4478.
[28] Xin X, Wang D, Han J, Feng Y, Feng Q, Chen W. Numerical optimization of a three-channel radiofrequency coil for open, vertical-field, MR-guided, focused ultrasound surgery using the hybrid method of moment/finite difference time domain method. NMR Biomed 2012; 25: 909–916.
[29] Xin SX, Huang Q, Gao Y, Li B, Xu Y, Chen W. Fetus MRI at 7 T: Shimming Strategy and SAR safety implications. IEEE Trans Microw Theory Tech 2013; 61: 2146–2152.
[30] Yang QX, Mao W, Wang J, et al. Manipulation of image intensity distribution at 7.0 T: Passive RF shimming and focusing with dielectric materials. J Magn Reson Imaging 2006; 24: 197–202.
[31] Yang QX, Wang J, Wang J, Collins CM, Wang C, Smith MB. Reducing SAR and enhancing cerebral signal-to-noise ratio with high permittivity padding at 3 T. Magn Reson Med 2011; 65: 358–362.
[32] Yang QX, Rupprecht S, Luo W, et al. Radiofrequency field enhancement with high dielectric constant (HDC) pads in a receive array coil at 3.0T. J Magn Reson Imaging 2013; 38: 435–440.